

ARTICLE

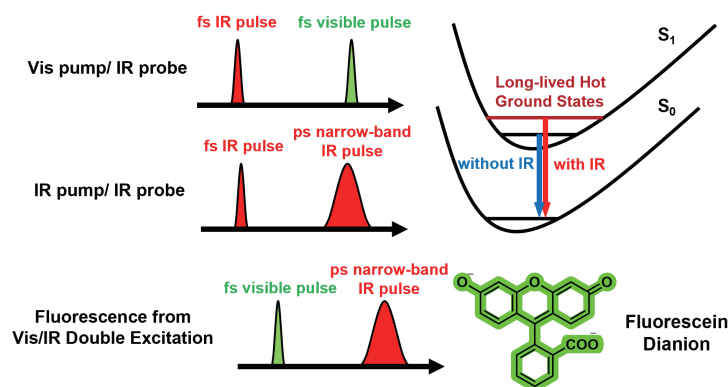
Direct Observation of Long-lived Vibrational Hot Ground States by Ultrafast Spectroscopy and Visible/Infrared Double Excitation Fluorescence[†]

Qirui Yu, Xinmao Li, Chengzhen Shen, Zhihao Yu, Jianxin Guan*, Junrong Zheng*

College of Chemistry and Molecular Engineering, Beijing National Laboratory for Molecular Sciences, Peking University, Beijing 100871, China

(Dated: Received on November 26, 2023; Accepted on March 8, 2024)

It is widely believed that the relaxation-induced bleaching signals at nanoseconds observed in ultrafast infrared spectroscopic measurements are due to the local heat effect resulting from the thermalization of the infrared excitations. In this work, combining ultrafast IR pump/probe, 2D-IR, visible pump/IR probe, and ultrafast visible/IR double resonant fluorescence experiments, the vibrational hot ground states of fluorescein dianion in methanol solutions are found to be unexpectedly long, at the time scale of nanoseconds. This result indicates that the long-standing bleaching signal observed in the nonlinear IR experiments must have significant contributions from these hot ground states for the initial couple of ns. It is likely that a similar mechanism can also hold for other molecular systems. The hot ground states can last much longer than conventionally expected, which can potentially be applied to modify chemical reactions.



Key words: Ultrafast spectroscopy, Fluorescence, Visible IR double excitation, Long-lived hot ground states, 2D-IR, Pump-probe

I. INTRODUCTION

Infrared excitation on molecular systems and materials can have a strong heating effect [1–11] on spectroscopic measurements. In a room temperature condensed sample, molecules absorb infrared photons and corresponding vibrations are excited. The vibrational excitations relax to lower vibrational energy levels and excite surrounding molecules by vibrational coupling

and energy transfer processes, typically at the time scales of a couple of picoseconds (ps) to hundreds of ps [5, 12–22]. The low-energy vibrational states, also named as hot ground states (HGS) [23, 24], will ultimately relax to the vibrational ground state by releasing heat to thermalize its local environment. The heat dissipation to the surrounding molecules to cause temperature rising locally [17] is called the local heat effect (LHE) [25, 26]. In many molecular systems, both hot ground states and the local heat effect redshift the 0-1 transition frequencies of high-frequency vibrational modes [7, 11, 13, 15, 16, 27, 28], making it difficult to distinguish the origins of experimentally observed frequency redshifts. In some cases, by comparing the temperature dependent FTIR absorption spectra with ul-

[†] Part of Special Issue “In Memory of Prof. Qihe Zhu on the occasion of his 100th Anniversary”.

* Authors to whom correspondence should be addressed. E-mail: guanjianxin1125@pku.edu.cn, junrong@pku.edu.cn, zhengjunrong@gmail.com

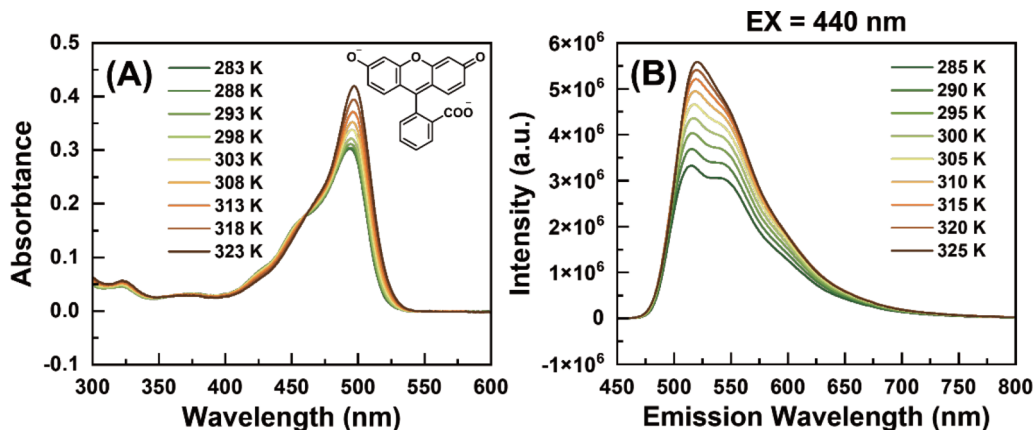


FIG. 1 (A) UV-visible absorption spectra and (B) fluorescence spectra by 440 nm excitation of 10^{-5} mol/L methanol solutions of fluorescein dianion (deprotonated by NaOH) at different temperatures. The molecular structure of fluorescein dianion is displayed as the insert in FIG. 1(A).

trafast pump/probe data, the temperature increase caused by the local heat effect can be estimated [17]. In general, most high-frequency vibrations and hot ground states are believed to have lifetimes ranging from a few ps up to hundreds of ps in a room temperature liquid, whereas the local heat effect can exist for longer than nanoseconds or even microseconds (μs) [9, 12, 22, 25, 26, 29–36]. For this sake, the observed frequency redshifts in ultrafast pump/probe or 2D-IR spectra at waiting times longer than 1 ns are generally assigned to the local heat effect without further experimental supports [9, 22, 28, 33].

It is the purpose of this work to investigate room temperature solutions at the time scale of ns if the hot ground states are insignificant as traditionally assumed. In order to achieve this goal, in addition to ultrafast pump/probe and 2D-IR measurements, fluorescence enhancement experiments by mode-selective vibrational excitation are also carried out.

Fluorescein dianion methanol solutions are chosen for this study. Fluorescein is known as one of the most common fluorescent probes because it has a very large absorption coefficient ε of $76900 \text{ mol}\cdot\text{L}^{-1}\cdot\text{cm}^{-1}$ at 490 nm and fluorescence quantum yield $\Phi > 90\%$ in aqueous solutions [37, 38]. Both factors contribute to its extremely high sensitivity as a fluorescent sensing probe. Fluorescein dianion can form dimers in protic solvents [37, 39–43]. The temperature-dependent UV-Vis absorption spectra and fluorescence spectra of its dilute solution are displayed in FIG. 1(A, B). With the increase of temperature, the monomer/dimer equilibrium shifts to more monomers, which partially contributes to increasing absorbance at 490 nm in FIG. 1(A) and slight redshift for fluorescence with en-

hanced intensity in FIG. 1(B). With the increase of concentration, the fluorescence emission redshifts to the dimer side significantly, shown in FIG. S2(A) in Supplementary materials (SM). The temperature dependence of fluorescence will serve as a critical parameter for the evaluation of individual contribution from the hot ground states and the local heat effect at long waiting times.

II. EXPERIMENTS

The ultrafast measurements were conducted with home-built systems which are introduced as follows. Details of measurements with routine techniques are provided in SM.

A. Ultrafast spectroscopy

The IR-pump/probe and 2D-IR studies were performed with a home-built fs/ps synchronized system [15, 44]. Briefly, laser pulses (1 kHz, ~ 50 fs pulse width, 800 nm central wavelength) from an amplified Ti/sapphire system (Uptek Solutions Inc.) are split into two beams. One beam is used to pump a femtosecond OPA (TOPAS), producing ~ 60 fs UV-visible pulses at 1 kHz, with a bandwidth of ~ 10 nm in a tunable frequency ranging from 250 nm to 800 nm. The visible beam excites the electron transition and the excitation power is $\sim 200 \mu\text{W}$ which is adjusted by an attenuator, with a spot diameter of $245 \mu\text{m}$. The other is used to pump another femtosecond OPA (Palitra, QUANTRONIX), producing pulses in a tunable frequency range from 1000 cm^{-1} to 3500 cm^{-1} at mid-IR region with a bandwidth $\sim 200 \text{ cm}^{-1}$ at 1 kHz. The mid-IR beam is used as the probe beam and detected by a 2×64 pixels mer-

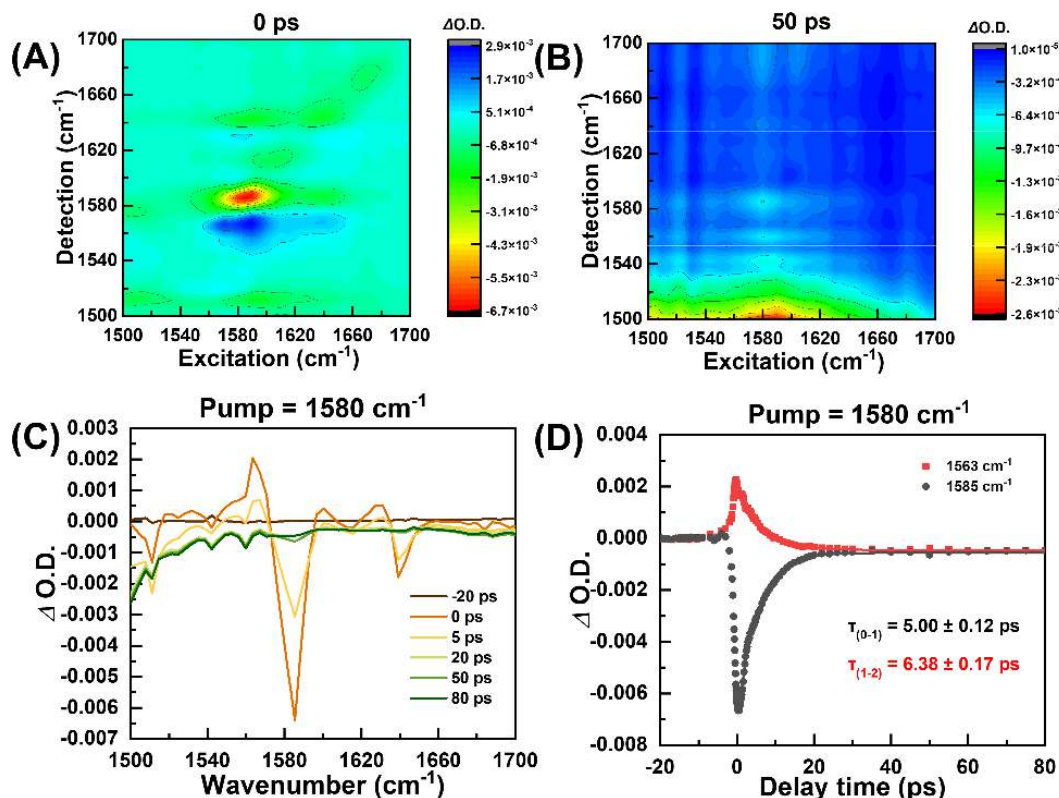


FIG. 2 (A, B) Normalized 2D-IR spectra of fluorescein dianion methanol solution. The time delays between pump and probe pulses are 0.1 ps and 50 ps. (C) 1580 cm^{-1} IR pump/IR probe spectra of fluorescein dianion methanol solution. The time delay between pump and probe pulses varied from -20 ps to 80 ps; (D) Time dependence of pump/probe signals with excitation at 1580 cm^{-1} and probed respectively at 1585 cm^{-1} and 1563 cm^{-1} . The time constants of the signal fast decay component are 5.0 ps and 6.4 ps respectively. The signal probed at 1563 cm^{-1} turns from absorption (positive) into bleaching (negative) at about 8 ps.

cury cadmium telluride (MCT) detector (Infrared associates) with a spectral resolution of ~ 3 cm^{-1} . The output (1 kHz, ~ 1.5 ps pulse width, 800 nm central wavelength) from a ps amplified Ti/sapphire laser system (Uptek Solutions Inc.) is used to pump a ps OPA (TOPAS), producing ~ 1 – 2 ps IR pulses ranging from 900 cm^{-1} to 3600 cm^{-1} with a bandwidth of ~ 10 – 20 cm^{-1} , serving as the narrow-band pump beam. Two polarizers are inserted into the mid-IR probe beam path. One is before the sample, which is used to rotate the polarization of the probe beam by 45° relative to that of the pump beam, and the other is located behind the sample in order to measure the parallel or vertical polarized signal relative to the pump beam selectively. Measuring the transmission of the mid-IR beam through the sample by chopping the pump beam to 500 Hz, the pump-probe signal $P(t)$ is collected and the vibrational lifetimes could be obtained from the rotation-free signal,

$$P(t) = \frac{1}{3} \left(P_{\parallel}(t) + 2P_{\perp}(t) \right)$$

where $P_{\parallel}(t)$ and $P_{\perp}(t)$ are the parallel and vertical sig-

nals, respectively.

The Vis-pump/IR-probe spectroscopic measurements are performed according to our previous report [45]. The fs visible laser is described as above, and the mid-IR output also serves as the probe beam.

B. Visible/IR double resonance fluorescence experiment

Briefly, the ps IR pulse spatially overlaps with the fs visible pulse on the sample surface, and the time delay between two pump pulses is controlled with a calibrated delay line. The wavelength-resolved fluorescence is collected into an optical fiber by an objective lens and sent to a spectrograph (Shamrock SR303i) equipped with an EMCCD (Newton EM, Andor DU970). The visible excitation power is 10 μW , and the integral time is ~ 50 s.

III. RESULTS AND DISCUSSION

A. Long-standing bleaching signals with infrared excitation

2D-IR spectra of the sample are measured, shown in

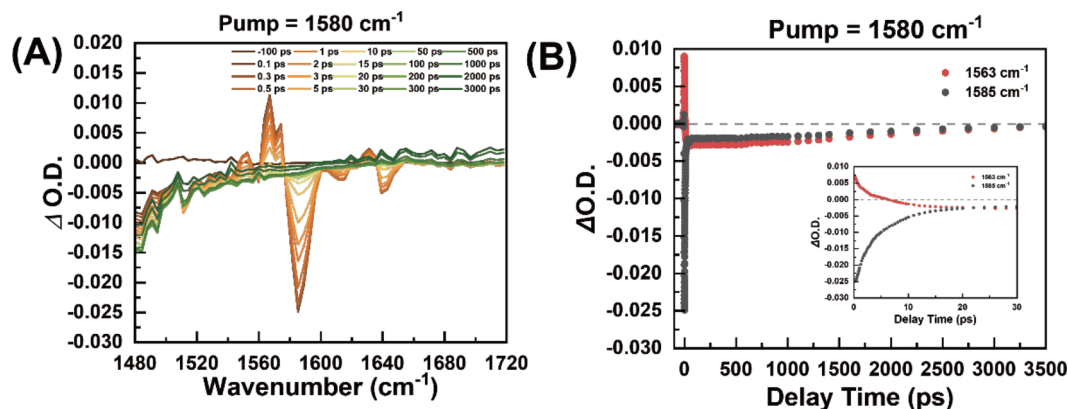


FIG. 3 (A) IR pump/probe spectra of the fluorescein dianion methanol solution with excitation at 1580 cm^{-1} . The extended range of time delay between pump and probe pulses is from -100 ps to 3500 ps ; (B) time dependence of pump/probe signal with excitation at 1580 cm^{-1} , and probed at 1585 cm^{-1} and 1563 cm^{-1} with waiting time up to 3.5 ns . The signal quickly changes from absorption into bleaching, and the bleaching signals for both probe wavenumbers last for more than 3.5 ns .

FIG. 2(A, B), and full spectra are provided in FIG. S5 (SM). By comparison with FTIR spectra and theoretical calculation results (FIG. S4 in SM), the bleaching and absorption peaks in the 2D-IR spectra can be assigned. In FIG. 2(A) with a very short waiting time of 0 ps , the red peak at 1580 cm^{-1} belongs to the $0-1$ transition of the xanthen skeleton stretch, and the blue peak with $\nu = 1563\text{ cm}^{-1}$ beneath it along the y -axis is its $1-2$ transition. The presence of off-diagonal peaks at $(1580\text{ cm}^{-1}, 1640\text{ and }1630\text{ cm}^{-1})$ and $(1640\text{ cm}^{-1}, 1580\text{ and }1563\text{ cm}^{-1})$ suggests that a xanthen ring stretch ($0-1$ transition frequency $\sim 1640\text{ cm}^{-1}$, shown in FIG. S4(D)) is coupled to the strongest skeleton stretch (FIG. S4(C) in SM). At a much longer time of 50 ps , the spectrum changes significantly, shown in FIG. 2(B). The absorption signals (blue peaks) diminish, whereas the bleaching signals (red peaks) become dominant. This change can be clearly seen in FIG. 2(C) which displays the time dependent spectra with excitation at 1580 cm^{-1} . In fact, both the bleaching and absorption peaks between 1540 cm^{-1} and 1640 cm^{-1} diminish very quickly. At 50 ps , all the absorption peaks disappear, and the bleaching peaks become very small and are replaced by a very broad bleaching signal that covers the entire range from 1500 cm^{-1} to 1700 cm^{-1} . The waiting time dependent pump/probe data with pump at 1580 cm^{-1} and probe at 1585 cm^{-1} are displayed in FIG. 2(D). The signal has a fast decay time constant of about 5 ps , and a very slow tail lasts more than 80 ps . Similar to many previous reports [7, 9, 13, 15, 36, 46, 47], the early decay of the bleaching signal is caused by the vibrational relaxation of the xanthen skeleton stretch with lifetime of 5 ps , whereas the slow rising

long tail results from the local heat effect, which is mainly from the dissipation of strong broadened methanol solvent vibration centered at $\sim 1400\text{ cm}^{-1}$ that can absorb 1580 cm^{-1} infrared photons, and the hot ground states. The waiting time dependent $1-2$ transition signal at 1563 cm^{-1} displayed in FIG. 2(D) behaves similarly. The absorption signal quickly decays with a time constant of 6.4 ps and at about 8 ps it turns into bleaching. Such a signal change can also be well explained with the same physical picture. Because the $1-2$ absorption signal is proportional to the population at the first vibrational excitation state of the xanthen skeleton stretch, once the population relaxes the absorption signal must diminish. The vibrational relaxation can also produce a local heat effect and hot ground states, which contribute to the bleaching signal following the disappearance of the absorption. The bleaching signal then decays very slowly along with the dissipation of hot ground states and the local heat effect. Up to 3.5 ns , the bleaching signal has not gone back to zero yet (FIG. 3(B)).

The waiting time dependent pump/probe spectra with excitation at 1580 cm^{-1} up to 3.5 ns are displayed in FIG. 3(A). As can be seen, up to 3.5 ns , the signal has not gone back to thermal equilibrium. The time dependent pump/probe signal with pump at 1580 cm^{-1} and probed at 1585 cm^{-1} in FIG. 3(B) clearly shows that the bleaching signal is yet to reach zero at 3.5 ns . All these results indicate that the relaxation of the fluorescein vibrational excitation at 1580 cm^{-1} generates hot ground states and local heat effect, mixed with the solvent local heat effect, leading to the appearance of the broad bleaching signal after the vibrational relaxation is com-

pleted (FIG. S6 in SM). As usual, one would expect that the hot ground states contribute dominantly within the initial a few hundred ps, and the local heat effect takes charge at longer waiting times as the hot ground states dissipate energy to the local environment. However, from the presented IR data, it is essentially impossible to confirm or disprove such a hypothesis. Other experimental evidence is needed to evaluate the lifetime of the hot ground states.

B. Blue-shifted and broadened fluorescence resulting from Visible/IR double excitations

Fluorescence encoded with vibrational information accomplished by visible/IR double resonances [48, 49] provides an opportunity to help resolve the difficulty mentioned above. In the experiments, the 540 nm visible pulse excites the molecules at the red edge of its UV-Vis absorption peak and the IR pulse is resonant with a certain vibrational mode. If the vibrational excitation can tremendously enhance the Franck-Condon factor [50–52], the double resonance can significantly enhance the total fluorescence intensity even if the number of molecules vibrationally excited is small compared to the total number of the sample. In our Vis/IR double resonant experiments with 540 nm and 1580 cm^{-1} excitations, the vibrationally excited molecules are over half of the total molecules (See SM part 10), whereas the fluorescence intensity from the double resonance is 2.6 times of that from excitation only by the 540 nm photons as shown in FIG. 4(A). Thus, the number of doubly excited molecules can be calculated to be a few times more than that only excited by the visible photons (see SM part 10 for calculation details), assuming that the vibrational excitation does not change the electronic transition dipole moment or energy dissipation pathways significantly.

It is very interesting that, in addition to the intensity enhancement, the fluorescence peak also blueshifts for 3.5 nm from 532.5 nm to 529.0 nm (FIG. 4(B)) compared to that with 540 nm excitation only. The blueshift is not caused by heating, since the results from temperature-dependent fluorescence spectra illustrate a significant redshift rather than blueshift of fluorescence at a higher temperature in FIG. 4(C). However, it would not be unreasonable to attribute such a blue shift to the sum frequency result. Photons with wavelength of $\sim 497\text{ nm}$ can be generated from the sum of pulses at

540 nm and 1580 cm^{-1} . Therefore, it is possible that the blueshift observed could be simply because the fluorescence with excitation at 497 nm is at a shorter wavelength compared to that excited with 540 nm. A shorter excitation wavelength does produce a fluorescence at a shorter wavelength, as displayed in FIG. 4(D). However, the linewidth change is different. In the double resonant experiment, the fluorescence linewidth is broadened by $\sim 0.2\text{ nm}$ (FIG. 4(E)), but the linewidth with 500 nm excitation is narrower than that with 540 nm excitation (FIG. 4(F)). Therefore, the results strongly suggest the peak blueshift and linewidth broadening are not because of the thermal effect nor the sum frequency effect. The possibility of sum result from both sum-frequency and heat effect is also excluded by the temperature-dependent fluorescence spectra with 500 nm excitation (FIG. S2(D) in SM).

According to the Kasha's rule, any photon emission, fluorescence or phosphorescence, occurs in appreciable yield only from the lowest excited state of a given multiplicity, because intramolecular vibrational relaxations (usually ps) are generally much faster than the photon emission processes (ns or slower) [53, 54]. Thus, excitations with 540 nm and 500 nm should produce very similar fluorescence spectra, if no other processes are involved. However, in the fluorescein solution, there is a dimer/monomer equilibrium. It is very likely that excitation with 500 nm can shift the equilibrium to the monomer side more than excitation with 540 nm, resulting in more emission from monomers of which the fluorescence has shorter wavelength compared to those of the dimers. Nevertheless, this explanation cannot apply to the fluorescence of double resonance as its linewidth is broadened. There is one remaining possibility. If the emission of the double resonant experiment is from the vibrational excited states rather than the vibrational ground state of the electronic excited state, it will naturally produce fluorescence blueshift and linewidth broadening as experimentally observed in the double resonance experiment. Previous sub-ps time-resolved fluorescence experiments [55–57] have shown that at early times such as hundreds of fs the fluorescence is blueshifted and broadened, because at such a short time the vibrational excitations have not completely relaxed away. The fluorescence is the emission from the vibrational excited states.

In our experiments, the fluorescence spectra of double resonance are detected with an EMCCD with a da-

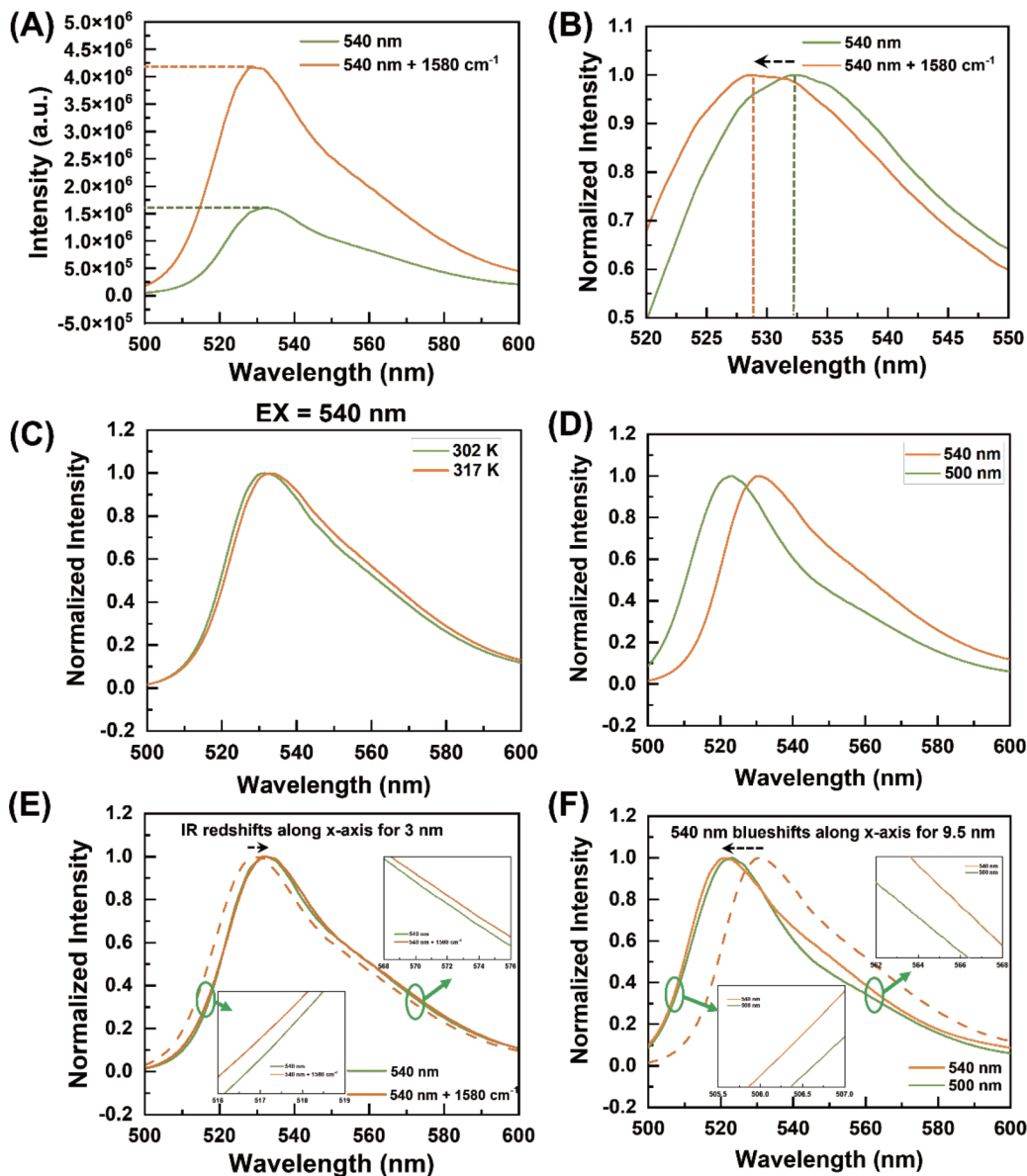


FIG. 4 (A) Fluorescence emission spectra with 540 nm excitation (green) and with 540 nm visible/1580 cm^{-1} IR double excitation at 1 ps time delay (IR arrives earlier). (B) Normalized fluorescence spectra showing that the fluorescence from the double resonance blueshifts for 3 nm. FIG. 4(A, B, E) are extracted from FIG. S7 in SM. (C) Normalized temperature-dependent fluorescence spectra at 302 K and 317 K for 0.01 mol/L condensed solution by 540 nm excitation. Fluorescence redshift for 1.6 nm from 302 K to 317 K. (D) Normalized fluorescence spectra with excitations at 500 nm (green) and 540 nm. (E) Fluorescence linewidth comparison. The double excited emission spectrum is translated along the x -axis for 3.0 nm for visual aid, showing the linewidth is broadened by ~ 0.2 nm compared to that with excitation at 540 nm. (F) Fluorescence linewidth comparison. The emission spectrum with 540 nm excitation is translated along the x -axis for 9.5 nm for visual aid, showing that the linewidth is significantly narrower with a shorter excitation wavelength.

ta acquisition time much longer than the fluorescence lifetime of the sample (about 4 ns, shown in FIG. S3 in SM), which means that the fluorescence intensity detected is the emission sum of all molecules electronically excited. To produce a noticeable blueshift, the lifetime of vibrational excitations must be comparable to that of the fluorescence lifetime. For heuristic purpose, a simple simulation assuming two Gaussians overlap-

ping with the same linewidth of 40 nm with different central wavelengths and intensity ratio is conducted and the result is discussed in the following. The fraction R of molecules which fluoresce directly from high vibrational levels is equal to:

$$R = \frac{k_{\text{rh}}}{k_{\text{rh}} + k_{\text{vib}}} \quad (1)$$

where k_{th} and k_{vib} are the rate constants of fluorescence emission directly from higher vibrational energy levels and vibrational relaxations respectively. $1/k_{\text{th}}$ here is approximately equal to the lifetime of fluorescence without IR excitation since the values of energy gaps are similar. In a condensed phase, $1/k_{\text{th}}$ (typically at the time scale of ns to tens of ns) is much longer than $1/k_{\text{vib}}$ (typically at the time scale of ps), which leads to $R \approx 0$, showing that very little fluorescence emission directly from high vibrational level exists. However, in order to produce the significant 3.5 nm blueshift observed in experiments (actually, the shift from the doubly excited molecules must be about 4 nm, considering the molecular ratio of double-excited/visible-excited. See SM part 11 for details), k_{vib} must be equivalent or even smaller than k_{th} . We can assume that the vibrational mode with energy of 142 cm^{-1} (the same energy as the 4 nm blueshift from 1/528.5–1/532.5 nm) has k_{vib} as large as k_{th} , then its lifetime is $\sim 4 \text{ ns}$, approximately the same as the fluorescence. Without knowing the ratio of fluorescence intensity, doubling the vibrational frequency to 284 cm^{-1} means only half of the blueshift photons are needed to provide the 3.5 nm blueshift. Thus, R reduces to its half, which leads $1/k_{\text{vib}}$ to become $\sim 1.4 \text{ ns}$, and the lifetime is $\sim 600 \text{ ps}$ if the vibrational frequency is 568 cm^{-1} . Even if the vibrational frequency is the same as the excitational 1580 cm^{-1} , R will reduce to 10%, and the required lifetime should be $\sim 200 \text{ ps}$. In other words, the observed fluorescence blueshift indicates that some low frequency vibrational excitations (hot ground states) resulted from the relaxation of 1580 cm^{-1} excitation must last very long, comparable to that of the fluorescence lifetime. Therefore, the long-standing bleaching signal observed in the IR pump/probe and 2D-IR data presented in FIG. 2 and FIG. 3 must have significant contributions from the hot ground states, at least for the initial couple of ns.

The lifetimes of these hot ground states are unexpectedly long. Two likely origins are discussed as follows. In their transition frequency range ($100\text{--}300 \text{ cm}^{-1}$), the solvent has plenty of resonant and quasi-resonant energy acceptor for them to dissipate energy. According to the dephasing energy transfer theory [58, 59], the coupling strength between the dark modes and the solvent accepting modes must be smaller than 0.1 cm^{-1} in order for the intermolecular energy transfer to be slower than 1 ns. In other words, the transition dipole moments of the dark modes must be very small,

and essentially, they must be Raman active rather than IR active and they acquire energy from the 1580 cm^{-1} excitation through mechanical coupling rather than dipole-dipole coupling. Besides, there is another possibility for these modes to be so long lived. As known from probing the solvent response at 1480 cm^{-1} (SM), the local effect generated in solvent has not been thermalized within a few ns. It is very likely that the heated solvent molecules have excited modes in the same frequency range, which release energy at the rate of heat dissipation (ns to tens of ns or even slower). These solvent modes are under fast energy exchange equilibrium with the hot ground states of fluorescein, which makes the hot ground states last long.

C. No high electronic excited states are involved

Visible pump/IR probe measurements are conducted to explore if other processes are involved, shown in FIG. 5 and FIG. S9 (SM). The time dependent pump/probe data with 540 nm excitation and probed at 1585 cm^{-1} are displayed in FIG. 5(A). The signal decay is a bi-exponential with time constants of 55 ps and 3595 ps with an amplitude ratio $\sim 0.14:1$. The fast component is probably caused by the solvation reorganization which usually has a timescale shorter than 100 ps [60]. The slow process has a time constant similar to the fluorescence lifetime of $\sim 4 \text{ ns}$ (FIG. S3 in SM), likely reflecting the decay of electronic excitation. By varying the excitation wavelength from 540 nm to 500 nm, similar peaks' positions and shapes are observed (FIG. 5(B)), indicating that the excited molecules probably reach the same electronic excited state, as higher electron excited states may have different effects on the vibrational frequencies. Thus, it is very likely that the doubly excited molecules fluoresce from higher vibrational states of the same electron excited state, rather than some higher electron excited states.

IV. CONCLUDING REMARKS

In summary, combining ultrafast IR pump/probe, 2D-IR, visible pump/IR probe, and ultrafast visible/IR double resonant fluorescence experiments, the hot vibrational ground states of fluorescein dianion in methanol solutions are found to be unexpectedly long, at the time scale of ns. This result indicates that the long-standing bleaching signal observed in the nonlinear IR experiments must have significant contributions from these hot ground states for the initial couple of ns.

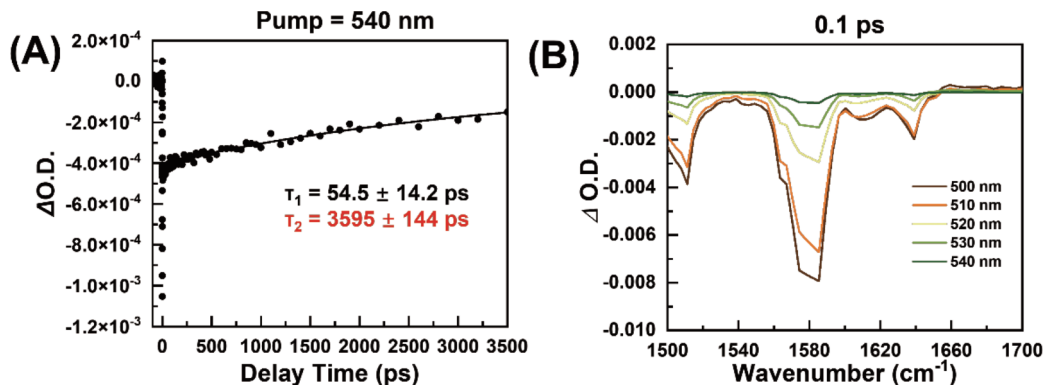


FIG. 5 (A) The signal decay of 540 nm visible pump/1585 cm^{-1} IR probe fit by double exponential model. (B) Visible pump/IR probe spectra at 0.1 ps time delay (IR arrives earlier) with excitation wavelength varying from 540 nm to 500 nm; the similar peaks' position and shapes suggest that fluorescein molecules reached the same electron state under different excitation wavelength.

It is likely that a similar mechanism can also hold for other molecular systems. The hot ground states can be much longer than conventionally expected.

Supplementary materials: Materials and methods; Experimental setup; FTIR spectrum; concentration, thickness and temperature-dependent fluorescence emission spectra; Fluorescence lifetime; IR spectra by theoretical calculation; 2D-IR spectra of fluorescein dianion methanol solution; visible/IR double excitation results; an estimation to the number of double-excited molecules; simulation results of Gaussians overlapping; visible pump/ IR probe results; calculation results and vibrations modes animation are available.

V. AUTHOR CONTRIBUTIONS

Qirui Yu, Jianxin Guan, and Junrong Zheng designed experiments. Jianxin Guan and Junrong Zheng supervised the project. Qirui Yu prepared materials and performed spectroscopy experiments. Qirui Yu, Xinmao Li, Jianxin Guan and Zhihao Yu performed ultrafast experiments. Qirui Yu, Xinmao Li, Jianxin Guan, Zhihao Yu and Junrong Zheng analyzed data. Qirui Yu and Chengzhen Shen conducted theoretical calculations. Qirui Yu, Jianxin Guan, and Junrong Zheng prepared and revised the manuscript.

VI. ACKNOWLEDGEMENTS

This work is by the National Natural Science Foundation of China (No.22203006, No.21927901, No.92261206, No.21627805, No.12174012, No.21673004, No.21821004, No.21674001, and No.21790363), Ministry of Science and Technology of China (a special tal-

ent program), and the Beijing City. We also thank the support from the High-performance Computing Platform of Peking University for the computational resources.

- [1] M. N. Slyadnev, Y. Tanaka, M. Tokeshi, and T. Kitamori, *Anal. Chem.* **73**, 4037 (2001).
- [2] A. C. Thompson, S. A. Wade, P. J. Cadusch, W. G. A. Brown, and P. R. Stoddart, *J. Biomed. Opt.* **18**, 035004 (2013).
- [3] R. W. Yu, A. Manjavacas, and F. J. García de Abajo, *Nat. Commun.* **8**, 2 (2017).
- [4] D. J. Hoffman, S. M. Fica-Contreras, J. K. Pan, and M. D. Fayer, *J. Chem. Phys.* **153**, 204201 (2020).
- [5] I. V. Rubtsov and A. L. Burin, *J. Chem. Phys.* **150**, 020901 (2019).
- [6] C. Lim, J. Jeon, K. Park, C. Liang, Y. Chae, K. Kwak, and M. Cho, *J. Phys. Chem. B* **127**, 9566 (2023).
- [7] Z. W. Lin, P. Keiffer, and I. V. Rubtsov, *J. Phys. Chem. B* **115**, 5347 (2011).
- [8] H. T. Bian, X. W. Wen, J. B. Li, and J. R. Zheng, *J. Chem. Phys.* **133**, 034505 (2010).
- [9] H. L. Chen, H. T. Bian, J. B. Li, X. W. Wen, and J. R. Zheng, *J. Phys. Chem. A* **117**, 6052 (2013).
- [10] J. B. Li, H. F. Qian, H. L. Chen, Z. Zhao, K. J. Yuan, G. X. Chen, A. Miranda, X. M. Guo, Y. J. Chen, N. F. Zheng, M. S. Wong and J. R. Zheng, *Nat. Commun.* **7**, 10749 (2016).
- [11] J. B. Li, Y. F. Zhang, and J. R. Zheng, *Phys. Chem. Chem. Phys.* **21**, 4240 (2019).
- [12] H. J. Bakker, P. C. M. Planken, and A. Lagendijk, *Nature* **347**, 745 (1990).
- [13] H. T. Bian, W. Zhao, and J. R. Zheng, *J. Chem. Phys.* **131**, 124501 (2009).

- [14] D. D. Dlott, *Chem. Phys.* **266**, 149 (2001).
- [15] Z. W. Lin and I. V. Rubtsov, *Proc. Natl. Acad. Sci. USA* **109**, 1413 (2012).
- [16] V. M. Kasyanenko, S. L. Tesar, G. I. Rubtsov, A. L. Burin, and I. V. Rubtsov, *J. Phys. Chem. B* **115**, 11063 (2011).
- [17] T. Steinel, J. B. Asbury, J. R. Zheng, and M. D. Fayer, *J. Phys. Chem. A* **108**, 10957 (2004).
- [18] P. Hamm, J. Helbing, and J. Bredenbeck, *Annu. Rev. Phys. Chem.* **59**, 291 (2008).
- [19] M. J. Feng, F. Yang, and J. P. Wang, *Chin. J. Chem. Phys.* **29**, 81 (2016).
- [20] Y. N. Shen, B. Jiang, C. Q. Ge, G. H. Deng, H. L. Chen, X. M. Yang, K. J. Yuan, and J. R. Zheng, *Chin. J. Chem. Phys.* **29**, 407 (2016).
- [21] F. Yang, P. Y. Yu, J. P. Shi, J. Zhao, X. M. He, and J. P. Wang, *Chin. J. Chem. Phys.* **26**, 721 (2013).
- [22] D. X. Zhou, Q. S. Wei, H. T. Bian, and J. R. Zheng, *Chin. J. Chem. Phys.* **30**, 619 (2017).
- [23] W. Frey and T. Elsaesser, *Chem. Phys. Lett.* **189**, 565 (1992).
- [24] S. A. Kovalenko, R. Schanz, H. Hennig, and N. P. Ernsting, *J. Chem. Phys.* **115**, 3256 (2001).
- [25] M. Cho, *J. Chem. Phys.* **157**, 124201 (2022).
- [26] L. M. Kiefer and K. J. Kubarych, *Coord. Chem. Rev.* **372**, 153 (2018).
- [27] D. V. Kurochkin, S. R. G. Naraharisetty, and I. V. Rubtsov, *Proc. Natl. Acad. Sci. USA* **104**, 14209 (2007).
- [28] K. P. Sokolowsky and M. D. Fayer, *J. Phys. Chem. B* **117**, 15060 (2013).
- [29] B. N. J. Persson and M. Persson, *Solid State Commun.* **36**, 175 (1980).
- [30] S. M. Fica-Contreras, R. Daniels, O. Yassin, D. J. Hoffman, J. K. Pan, G. Sotzing, and M. D. Fayer, *J. Phys. Chem. B* **125**, 8907 (2021).
- [31] F. Chalyavi, A. J. Schmitz, N. R. Fetto, M. J. Tucker, S. H. Brewer, and E. E. Fenlon, *Phys. Chem. Chem. Phys.* **22**, 18007 (2020).
- [32] D. Kossowska, K. Park, J. Y. Park, C. Lim, K. Kwak, and M. Cho, *J. Phys. Chem. B* **123**, 6274 (2019).
- [33] Y. L. A. Rezus and H. J. Bakker, *J. Chem. Phys.* **123**, 114502 (2005).
- [34] H. T. Bian, H. L. Chen, J. B. Li, X. W. Wen, and J. R. Zheng, *J. Phys. Chem. A* **115**, 11657 (2011).
- [35] L. J. G. W. van Wilderen, D. Kern-Michler, H. M. Müller-Werkmeister, and J. Bredenbeck, *Phys. Chem. Chem. Phys.* **16**, 19643 (2014).
- [36] J. Bredenbeck, J. Helbing, A. Sieg, T. Schrader, W. Zinth, C. Renner, R. Behrendt, L. Moroder, J. Wachtveitl, and P. Hamm, *Proc. Natl. Acad. Sci. USA* **100**, 6452 (2003).
- [37] I. L. Arbeloa, *J. Chem. Soc. Faraday Trans. 2: Mol. Chem. Phys.* **77**, 1725 (1981).
- [38] R. Sjöback, J. Nygren, and M. Kubista, *Spectrochim. Acta Part A: Mol. Biomol. Spectrosc.* **51**, L7 (1995).
- [39] F. L. Arbeloa, P. R. Ojeda, and I. L. Arbeloa, *J. Chem. Soc., Faraday Trans. 2: Mol. Chem. Phys.* **84**, 1903 (1988).
- [40] I. L. Arbeloa, *J. Chem. Soc. Faraday Trans. 2: Mol. Chem. Phys.* **77**, 1735 (1981).
- [41] T. Casalini, M. Salvalaglio, G. Perale, M. Masi, and C. Cavallotti, *J. Phys. Chem. B* **115**, 12896 (2011).
- [42] S. Speiser, V. H. Houlding, and J. T. Yardley, *Appl. Phys. B* **45**, 237 (1988).
- [43] S. De, S. Das, and A. Girigoswami, *Spectrochim. Acta Part A: Mol. Biomol. Spectrosc.* **61**, 1821 (2005).
- [44] H. L. Chen, H. T. Bian, J. B. Li, X. W. Wen, and J. R. Zheng, *Int. Rev. Phys. Chem.* **31**, 469 (2012).
- [45] J. X. Guan, R. Wei, A. Prlj, J. Peng, K. H. Lin, J. T. Liu, H. Han, C. Corminboeuf, D. H. Zhao, Z. H. Yu, and J. R. Zheng, *Angew. Chem. Int. Ed.* **132**, 14903 (2020).
- [46] S. Woutersen, U. Emmerichs, and H. J. Bakker, *Science* **278**, 658 (1997).
- [47] M. F. Kropman and H. J. Bakker, *J. Chem. Phys.* **115**, 8942 (2001).
- [48] H. M. Wang, D. Lee, Y. L. Cao, X. T. Bi, J. J. Du, K. Miao, and L. Wei, *Nat. Photonics* **17**, 846 (2023).
- [49] L. Whaley-Mayda, A. Guha, S. B. Penwell, and A. Tokmakoff, *J. Am. Chem. Soc.* **143**, 3060 (2021).
- [50] J. von Cosel, J. Cerezo, D. Kern-Michler, C. Neumann, L. J. G. W. van Wilderen, J. Bredenbeck, F. Santoro, and I. Burghardt, *J. Chem. Phys.* **147**, 164116 (2017).
- [51] E. U. Condon, *Am. J. Phys.* **15**, 365 (1947).
- [52] J. Bredenbeck, J. Helbing, and P. Hamm, *J. Am. Chem. Soc.* **126**, 990 (2004).
- [53] M. Kasha, *Discuss. Faraday Soc.* **9**, 14 (1950).
- [54] M. Kasha, H. R. Rawls, and M. A. El-Bayoumi, *Pure Appl. Chem.* **11**, 371 (1965).
- [55] A. Cannizzo, F. van Mourik, W. Gawelda, G. Zgrablic, C. Bressler, and M. Chergui, *Angew. Chem. Int. Ed.* **45**, 3174 (2006).
- [56] A. Mokhtari, J. Chesnoy, and A. Laubereau, *Chem. Phys. Lett.* **155**, 593 (1989).
- [57] R. Schanz, S. A. Kovalenko, V. Kharlanov, and N. P. Ernsting, *Appl. Phys. Lett.* **79**, 566 (2001).
- [58] H. L. Chen, H. T. Bian, J. B. Li, X. W. Wen, Q. Zhang, W. Zhuang, and J. R. Zheng, *J. Phys. Chem. B* **119**, 4333 (2015).
- [59] H. L. Chen, X. W. Wen, X. M. Guo, and J. R. Zheng, *Phys. Chem. Chem. Phys.* **16**, 13995 (2014).
- [60] J. R. Lakowicz, *Principles of Fluorescence Spectroscopy*, New York: Springer, (2006).